

Saddle stresses for generic theories with a preferred acceleration scale

João Magueijo^{1,*} and Ali Mozaffari^{1,†}

¹*Theoretical Physics, Blackett Laboratory, Imperial College, London, SW7 2BZ, United Kingdom*
(Dated: March 3, 2013)

We show how scaling arguments may be used to generate templates for the tidal stresses around saddles for a vast class of MONDian theories *detached from their obligations as dark matter alternatives*. Such theories are to be seen simply as alternative theories of gravity with a preferred acceleration scale, and could be tested in the solar system by extending the LISA Pathfinder (LPF) mission. The constraints thus obtained may then be combined, if one wishes, with requirements arising from astrophysical and cosmological applications, but a clear separation of the issues is achieved. The central technical content of this paper is the derivation of a scaling prescription allowing complex numerical work to be bypassed in the generation of templates. We find that LPF could constrain very tightly the acceleration a_0 and the free parameter κ present in these theories. As an application of our technique we also produce predictions for the moon saddle (for which a similar scaling argument is applicable) with the result that we recommend that it should be included in orbit design.

I. INTRODUCTION

There is an ubiquitous acceleration scale in the universe, $a_0 \sim 10^{-10} \text{ ms}^{-2}$, which turns up variously in cosmology and astrophysics: the cosmic expansion rate, galactic rotation curves, etc. This observation has prompted the investigation of alternative theories of gravity endowed with a preferred acceleration. TeVeS [1], and more generally relativistic MONDian theories [2–6], provide a blueprint for such constructions. MONDian theories were first proposed with the motivation of bypassing the need for dark matter [7, 8]. However, they may also be considered independently from this application, and be seen simply as alternative theories of gravity [9] into which an acceleration scale has been embedded. In this guise they constitute prime targets for experimental gravitational tests inside the solar system.

As an example let us consider TeVeS (but what follows applies generally to what in [10] was labelled “Type I” theories). Abstracting from aspects which do not affect the non-relativistic limit, the theory benefits from the leeway of a whole free-function μ . Its choice may be informed by minimalism and simplicity, e.g. μ may be built to encode only 2, rather than 3 or more regimes. Putting aside details affecting the transition between the two regimes, we are then left with two free parameters: a_0 (the acceleration scale of the theory) and κ (controlling the renormalization of the gravitational constant G). These are fixed by astrophysical and cosmological applications, if the theory is to act as a competitor to dark matter. But a_0 and κ can also be seen as fully free parameters in any solar system test.

Specifically, these theories predict a rich phenomenology around the saddle points of the gravitational potential. The prospect of extending the LISA Pathfinder

mission so that a saddle of the Sun-Earth-Moon system is visited brings them within experimental striking range [10–15]. Predictions for minimal theories constrained by cosmological and astrophysical applications were studied in [10], where the general impact of a negative result was also examined. Detaching the target theory from its duties as “dark matter” alternative requires the generation of a large database of templates. However, re-running the adaptive-mesh code presented in [11] for each μ is simply not feasible, and we run up against a computational wall.

In this paper we show how this work can be partly alleviated. As long as we are interested in changing only κ and a_0 , a simple scaling argument allows the generation of the whole set of required templates from those obtained with fiducial values for a_0 and κ , shortcutting tedious or downright impossible hard labour. The analytical argument is laid down in Section II, and its application to LPF is given in Section III. In order to include another topical application, in Section IV we also show how the lunar saddle would fare, were LPF to include it in a mission extension.

II. SCALING BEHAVIOUR AROUND SADDLES

Scaling is an interesting tool for generating solutions to apparently intractable problems. For example imposing a self-similar ansatz leads to striking progress in the study of gravitational collapse, rendering what *a priori* are PDEs into simpler ODEs (e.g. [16, 17]). Scaling behaviour was observed in the MONDian tidal stresses around saddles, when comparing the profiles around the Moon saddle and the Earth-Sun saddle (see Fig. 12 in [11], and its surrounding comments). It was noted that the tidal stresses are very approximately the same once they are spatially stretched and their amplitude scaled to account for the different Newtonian tidal stress A . In what follows we rigorously explain this empirical fact and extend its scope, deriving the scaling laws associated with

*Electronic address: magueijo@ic.ac.uk

†Electronic address: ali.mozaffari05@ic.ac.uk

varying a_0 and κ .

In TeVeS and other type I theories [10] the non-relativistic dynamics results from the joint action of the usual Newtonian potential Φ_N (associated with the metric) and a “fifth force” scalar field, ϕ , responsible for MONDian effects. The total potential acting on non-relativistic particles is their sum $\Phi = \Phi_N + \phi$. The field ϕ is ruled by a non-linear Poisson equation:

$$\nabla \cdot (\mu(z) \nabla \phi) = \kappa G \rho, \quad (1)$$

with $z = \frac{\kappa}{4\pi} \frac{|\nabla \phi|}{a_0}$. Here κ is a dimensionless constant and a_0 is the usual MONDian acceleration.

For these theories, the argument presented in Sections II and IV of [12], for a specific μ , can be generalized for any μ . It is always possible to define a variable:

$$\mathbf{U} = -\frac{\kappa}{4\pi a_0} \mu(z) \nabla \phi \quad (2)$$

in terms of which the vacuum equations become:

$$\nabla \cdot \mathbf{U} = 0 \quad (3)$$

$$\alpha(U) U^2 \nabla \wedge \mathbf{U} + \mathbf{U} \wedge \nabla U^2 = 0, \quad (4)$$

i.e. the free parameters a_0 and κ drop out, and “universal” equations are obtained. Here

$$\alpha(U) = \frac{d \ln U^2}{d \ln \mu}, \quad (5)$$

(notice that $U^2 = z^2 \mu^2(z)$, so that μ can be written as a function of U alone, $\mu = \mu(U)$). The MONDian physical force can be obtained from \mathbf{U} using:

$$\mathbf{F}_\phi = -\nabla \phi = \frac{4\pi a_0}{k} \frac{1}{\mu(U)} \mathbf{U}, \quad (6)$$

which follows directly from (2). In [12] the choice was made:

$$\mu = \frac{U^{1/2}}{(1 + U^2)^{1/4}} \quad (7)$$

so that $\alpha = 4(1 + U^2)$, in agreement with Eqns. (30)-(31) of [12], and

$$\mathbf{F}_\phi = -\nabla \phi = \frac{4\pi a_0}{k} (1 + U^2)^{1/4} \frac{\mathbf{U}}{U^{1/2}}, \quad (8)$$

in agreement with Eqn. 32 in [12]. However, as we see, the argument can be adapted to any function μ .

Equations (3) and (4) are invariant under a rigid rescaling of the spatial variables:

$$\mathbf{U} \rightarrow \mathbf{U} \quad (9)$$

$$\mathbf{x} \rightarrow \lambda \mathbf{x} \quad (10)$$

where λ is spatially constant. To use the technical term they admit homothetic solutions, i.e.:

$$\mathbf{U} = \mathbf{F}(\lambda \mathbf{x}). \quad (11)$$

where \mathbf{F} is a universal function. However, we have yet to supply Equations (3) and (4) with boundary conditions. This is done by going far enough from the saddle so that the field ϕ has entered the Newtonian regime. With the conventions used in [10] one has $\mu \rightarrow 1$ (the renormalization in G is fully absorbed in κ), and so:

$$\phi \approx \frac{\kappa}{4\pi} \Phi_N. \quad (12)$$

The appropriate boundary condition is then supplied from the Newtonian limit relation:

$$\mathbf{U} \approx \frac{\kappa}{4\pi a_0} \mathbf{F}_\phi \approx \left(\frac{\kappa}{4\pi}\right)^2 \frac{1}{a_0} \mathbf{F}_N. \quad (13)$$

Let us first assume that we can approximate the Newtonian field around the saddle as a linear function, for the purpose of effectuating this matching. Then:

$$\mathbf{F}_N = -\nabla \Phi_N = A r \mathbf{N}(\theta, \phi), \quad (14)$$

where A is the Newtonian tidal stress at the saddle point, and \mathbf{N} is its angular profile (see Eqs. 35-37 in [12]). Defining the MONDian “bubble size” as usual:

$$r_0 = \frac{16\pi^2 a_0}{\kappa^2 A} \quad (15)$$

we therefore have in the Newtonian regime and close enough to the saddle:

$$\mathbf{U} \approx \frac{r}{r_0} \mathbf{N}(\theta, \phi). \quad (16)$$

This boundary condition allows us to select the homothetic solution (11) appropriate to a given saddle and free parameters. To match the boundary conditions one should set $\lambda = 1/r_0$, so that the solution is

$$\mathbf{U} = \mathbf{F}\left(\frac{\mathbf{x}}{r_0}\right). \quad (17)$$

The above argument is still (approximately) valid if one goes beyond the linear approximation, as long as this approximation is good up to a few r_0 . If the parameters a_0 and κ lead to a breakdown of this assumption, however, then scaling is lost.

We can now read off similar scaling laws for more familiar quantities. Using (8) we see that the MONDian force must have the form:

$$\mathbf{F}_\phi = \frac{a_0}{\kappa} \mathbf{G}\left(\frac{\mathbf{x}}{r_0}\right) \quad (18)$$

where \mathbf{G} is another universal function. (This scaling law is obvious by direct inspection of the analytical solutions derived for the μ used in [12]; however, as we now see, it is more general). By taking derivatives we then find that the MONDian tidal stresses must have the form

$$S_{ij} = \kappa A H_{ij} \left(\frac{\mathbf{x}}{r_0}\right) \quad (19)$$

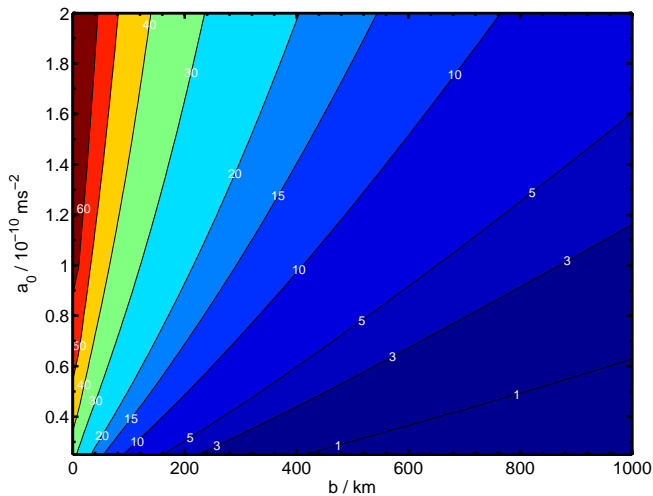


FIG. 1: The effect on the Signal-to-Noise Ratio (SNR) resulting from varying a_0 , assuming different impact parameters b and the best estimate for the noise at the time of writing (with κ kept fixed at $\kappa = 0.03$). The fiducial value used in previous publications is $a_0 = 10^{-10} \text{ ms}^{-2}$. Generally the larger the a_0 the higher the SNR.

where the H_{ij} are also universal. This explains the scaling law observed for different A , and fixed κ and a_0 , when comparing the Moon and Earth saddles [11]. But it also allows for templates for general values of κ and a_0 to be generated from those for fiducial values simply by rescaling them according to the above laws.

III. AN APPLICATION

The practical applications of the previous section are far-reaching and will be the subject of a number of future publications devoted to the data analysis of a saddle test. As a simple example we examine in this section the impact of a_0 and κ on the SNR (Signal to Noise Ratio) forecast for a LISA Pathfinder flyby. As in [10], we assume the use of an optimal noise-matched filter, using for our noise model the best estimate at the time of writing (labelled “Best Case Noise” in Fig.6 of [10]). We then inspect the SNR variations with a_0 and κ for different saddle impact parameters b . After a number of studies, following on from [13], an impact parameter $b \sim 10 - 50 \text{ km}$ is now considered realistic. Multiple flybys are currently being investigated, for which b may not be as good. We therefore consider SNRs for b up to 1000 km. Recall that for the fiducial values $a_0 = 10^{-10} \text{ ms}^{-2}$ and $\kappa = 0.03$ (required, or suggested, by cosmological and astrophysical applications) one forecasts SNRs for the Earth-Sun saddle around 40-60 for the expected $b = 10 - 50 \text{ km}$, only dropping below 5 beyond $b \sim 700 \text{ km}$ (see Fig.7 of [10]).

The effect of changing the acceleration scale a_0 is plotted in Fig. 1. It results from a change in the MOND bubble size r_0 , as predicted by Eqn. 15. Therefore the

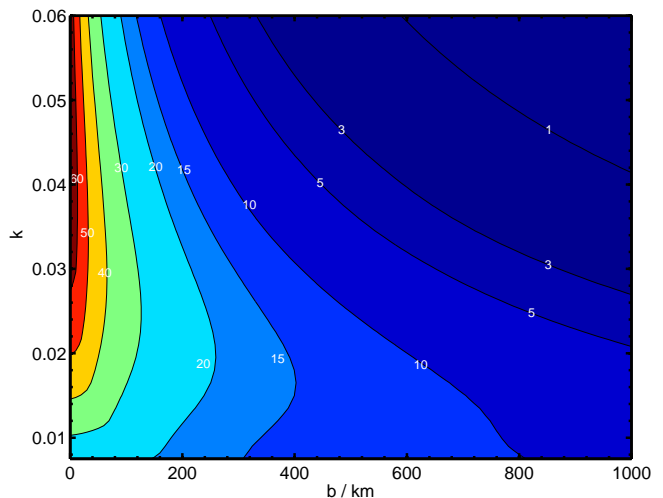


FIG. 2: Effect on the SNR obtained by varying κ (keeping a_0 fixed at the fiducial value). The fiducial value used in previous publications is $\kappa = 0.03$. At small b , changing κ may increase or decrease the SNR (see text for explanation). At large b one is better off with a small κ .

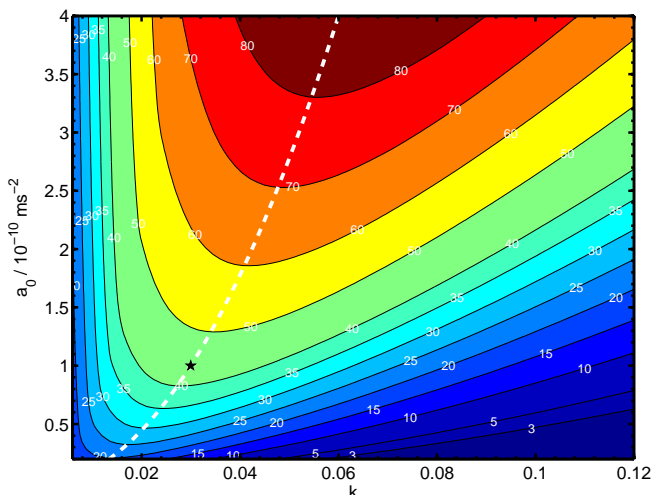


FIG. 3: Effect on SNR obtained by jointly varying a_0 and κ , for a trajectory with impact parameter $b = 50 \text{ km}$. The fiducial values have been indicated with a star. We also plot (dashed white line) the contour of constant r_0 passing through the fiducial values.

SNR is roughly constant on lines of constant b/a_0 . The slope of the iso-SNR lines is not constant and they are not exactly straight because the SNR algorithm is quite complicated and non-linear. We see that even at large b it is possible to turn a weak result into a strong positive one by increasing a_0 by a factor of 2. Conversely, if a_0 is halved, a SNR below ~ 5 is now a liability for b as low as $\sim 350 \text{ km}$. Without external constraints fixing a_0 to better than an order of magnitude, it is therefore risky to give up on a $b \sim 10 - 50 \text{ km}$.

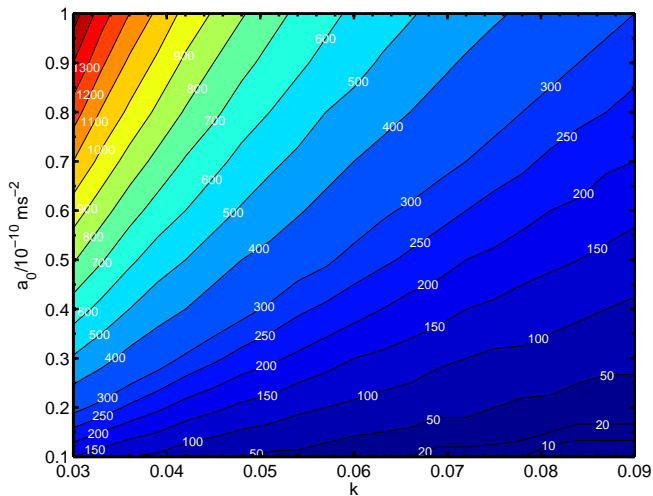


FIG. 4: Constraints placed on a_0 and κ by a negative result for different impact parameters b (labelling the lines and coding the colours). For a given b , the admissible parameter space would be “outside” the corresponding b line (i.e. towards the right lower corner).

The effect of changing κ is plotted in Fig. 2 and results from two sources: a change in bubble size according to $r_0 \propto 1/\kappa^2$ (cf. Eqn. 15) and an overall factor multiplying the amplitude (cf. Eqn. 19). The two effects counteract each other, so that unless b is very large, the SNR at first increases with κ , then decreases. For the expected $b \sim 10 - 50$ it can go either way. For large b (greater than $b \sim 500$ km for the fiducial value of a_0), the bubble size prevails and so the SNR decreases with increasing κ . The interplay of these two effects is best illustrated in Fig. 3, where we plotted the effect on the SNR of changing simultaneously a_0 and κ for fixed $b = 50$ km. We also plotted the line of constant r_0 passing through the fiducial values. As we see the SNR does change along this line, showing that the bubble size r_0 is not the only consideration.

Supposing we get a negative result, what constraints can we place upon a_0 and κ ? As in [10] we may get a preliminary estimate by seeking the region where the SNR for an optimal filter drops below 1. This was plotted Fig. 4 for various values of b (in this figure, b labels the lines and codes the colours). For a given b , the admissible parameter space is “outside” the corresponding b line (i.e. towards the right-bottom corner). In general, a negative result forces a_0 to be smaller and κ to be larger than the fiducial values, the more so, the smaller the impact parameter b . As we see, if we were to miss the saddle by 1500 km or more, the fiducial values of a_0 and κ would survive a negative result. For an approach any closer, however, a negative result would rule them out and squeeze the parameter space towards the right-bottom corner. For $b \sim 10$ km, the a_0 (the κ) would have to be smaller (larger) than the fiducial values by an order

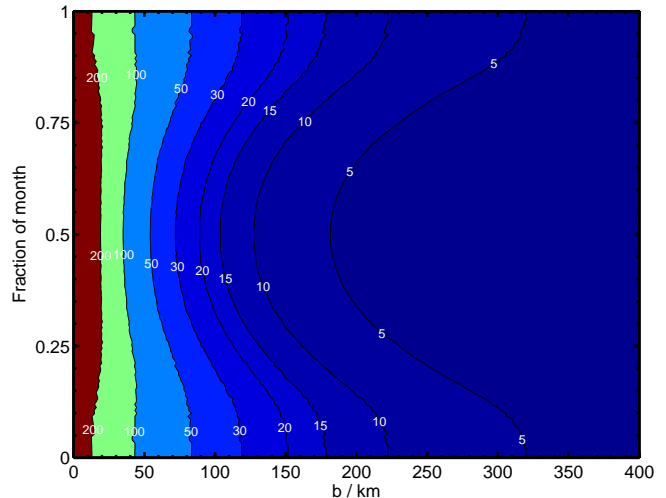


FIG. 5: SNRs for the moon saddle, assuming a standard noise model and speed $v = 0.3 \text{ km s}^{-1}$, for different impact parameters and day of the month (0 and 1 represent the New Moon, 0.5 the Full Moon). We see that the moon saddle is less forgiving if you miss it by more than 150 km and more rewarding if you get close to it (with SNRs of 200 within reach). If the former, new moons generate higher SNRs.

of magnitude.

These constraints may now be combined with other pressures upon the theory, such as those arising from limits on G renormalisation, Big Bang Nucleosynthesis, fifth force solar system tests, galaxy rotation curve data, and cosmological structure formation. However, as advocated in the introduction, by allowing complete freedom in a_0 and κ in a saddle test, we have achieved a clear separation of the issues confronting these theories.

IV. THE MOON SADDLE AS A LPF TARGET

Our technique can also be applied to a very topical issue: whether the Moon saddle is a good alternative target for LPF. Practical matters may render this saddle more amenable to multiple flybys, an issue that could be essential in dismissing a “false alarm”, should a positive detection be found. In the absence of a more detailed study of transfer orbits we evaluate SNR’s for the moon saddle, hoping that this may motivate further work in orbit design.

Application of the algorithm in Section II to the moon saddle is straightforward (and indeed it motivated the argument presented therein). As noted in [11], r_0 for the Moon saddle is smaller than the 380km found for the Earth-Sun saddle, and this size is more variable, depending strongly on the phase of the Moon (it varies between 25km and 80km; see Fig.10 of [11]). However A is larger, too, so the tidal stresses have a larger amplitude. Nevertheless, what really matters for SNRs is the Fourier

transform of the signal as seen in time, with the satellite going through the bubble. The large SNRs obtained for the Sun-Earth saddle result from a miraculous coincidence between the sweet spot in the amplitude spectral density (ASD), and the size of the bubble as transformed into a time-signal by the typical velocities found in transfer orbits. This miracle could be spoiled by the smaller size of the Moon saddle.

As it happens, orbits crossing the Moon saddle do so with a smaller velocity, typically smaller than 0.5 km s^{-1} . The two effects—smaller bubble, smaller speed—counteract each other when converting the bubble signal into a time signal. Therefore it is not surprising that the SNRs predicted for the Moon saddle are as high as those for the Earth saddle, albeit more variable in time, depending on the phase of the moon.

In Fig. 5 we plotted SNRs assuming the standard noise model we have used throughout this paper, for a crossing of the moon saddle at $v = 0.3 \text{ km s}^{-1}$, for different impact parameters and day of the month. On the y -axis 0 and 1 represent the New Moon, and 0.5 represents the Full Moon. As we can see, in comparison with the Earth-Sun saddle, the moon saddle:

- is less forgiving if you miss it by more than 150 km.
- is more rewarding if you get close to it (with SNRs of 200 within reach).
- in the first case, then the lunar phase is crucial, with the new moon producing the best results.

In view of these results we think we should urge the orbit designers to include the moon saddle in their considerations.

V. CONCLUSIONS

To conclude, we have presented a simple argument allowing the inference of a large database of templates for

¹ Steve Kemble, private communication

the tidal stresses that would be felt by LISA Pathfinder, should a saddle flyby be incorporated into the mission. The argument allows for the variation of the acceleration scale a_0 and κ . Should the functional form of the free function μ be changed, the SNRs obtained would change, but only as predicted in [10]: they wouldn't change much for MONDian two-regime functions, unless b is much larger than r_0 . We may detach these theories altogether from their “alternative to dark matter duties”. Then we may consider two-regime functions with $\mu \rightarrow 1$ at large arguments, but $\mu \propto z^n$, with $n \neq 1$, when z is small. The scaling argument presented here would still be applicable in this context, but the fiducial templates would have to be obtained by re-running a numerical code for each n . In a paper in preparation we show how this may be bypassed too, albeit with a much more complex analytical argument.

The practical applications of our technique are far-reaching and will be the support of a number of future publications concerned with the data analysis of a saddle test. In this paper we merely showed how SNRs change by changing the parameters of the theory. This gives an indication of how sensitive to them the experiment is, and therefore how much it will constrain them. More importantly, as an application we applied our scaling algorithm to the prediction of results for the Moon saddle. The results were very encouraging and lead us to urge the orbit designers to include it in their considerations.

Acknowledgments

We thank Pedro Ferreira and Steve Kemble for useful discussions as well as the whole LPF science team. AM is funded by an STFC studentship. All the numerical work was carried out on the COSMOS supercomputer, which is supported by STFC, HEFCE and SGI.

-
- [1] J. D. Bekenstein, Phys. Rev. **D70**, 083509 (2004); Erratum-ibid. **D71**, 069901 (2005), astro-ph/0403694.
 - [2] R. H. Sanders, Mon. Not. Roy. Astron. Soc. **363**, 459 (2005), astro-ph/0502222.
 - [3] T. G. Zlosnik, P. G. Ferreira, and G. D. Starkman, Phys. Rev. **D74**, 044037 (2006), gr-qc/0606039.
 - [4] T. G. Zlosnik, P. G. Ferreira, and G. D. Starkman, Phys. Rev. **D75**, 044017 (2007), astro-ph/0607411.
 - [5] M. Milgrom, Phys. Rev. **D80**, 123536 (2009), 0912.0790.
 - [6] M. Milgrom, Mon. Not. Roy. Astron. Soc. **405**, 1129 (2010), 1001.4444.
 - [7] M. Milgrom, Astrophys. J. **270**, 365 (1983).
 - [8] B. Famaey and S. McGaugh (2011), arXiv:1112.3960.
 - [9] T. Clifton, P. G. Ferreira, A. Padilla, and C. Skordis, Phys.Rept. **513**, 1 (2012), 1106.2476.
 - [10] J. Magueijo and A. Mozaffari, Phys.Rev. **D85**, 043527 (2012), 1107.1075.
 - [11] N. Bevis, J. Magueijo, C. Trenkel, and S. Kemble, Class. Quant. Grav. **27**, 215014 (2010), 0912.0710.
 - [12] J. Bekenstein and J. Magueijo, Phys. Rev. **D73**, 103513 (2006), astro-ph/0602266.
 - [13] C. Trenkel, S. Kemble, N. Bevis, and J. Magueijo (2010), 1001.1303.
 - [14] A. Mozaffari (2011), arXiv:1112.5443.
 - [15] P. Gialianni, M. Feix, H. Zhao, and K. Horne (2011), 1111.6681.
 - [16] E. Bertschinger, ApJS **58**, 1 (1985).
 - [17] E. Bertschinger, ApJS **58**, 39 (1985).